Silanes and Other Coupling Agents, Vol. 4, pp. 1–16
Ed. K.L. Mittal

Self-assembled monolayers of omega-functional silanes: A platform for understanding cellular adhesion at the molecular level

MARK H. LEE,[1,2,3,*] DAVID BOETTIGER,[1,3] PAUL DUCHEYNE[1,4] and RUSSELL J. COMPOSTO[1,2]

[1]*Institute for Medicine & Engineering, University of Pennsylvania, Philadelphia, PA 19104, USA*
[2]*Department of Materials Science & Engineering, University of Pennsylvania, Philadelphia, PA 19104, USA*
[3]*Department of Microbiology, University of Pennsylvania, Philadelphia, PA 19104, USA*
[4]*Department of Bioengineering, University of Pennsylvania, Philadelphia, PA 19104, USA*

Abstract—Self-assembly represents a powerful and versatile strategy to create substrates with controlled molecular-level physicochemical characteristics. As a result, self-assembled monolayers (SAMs) of silanes continue to find use in a multitude of applications in biotechnology and nanotechnology, both as model substrates to study interfacial interactions and as a strategy to chemically graft bioactive molecules. In our work, SAMs of various functional groups have been used for fundamental studies of cellular interactions with peptides and proteins. Namely, cellular adhesion was quantitatively probed to elucidate the roles of non-specific forces arising from the substrate and to study the specific interactions of cellular receptors with adsorbed extracellular matrix (ECM) proteins, such as fibronectin, and grafted arginine–glycine–aspartic acid (RGD) peptides. Measurements of the cellular detachment strength using a spinning disc apparatus demonstrated that the terminal functionality of the silane SAM used as the substrate exerted significant effects and highlighted the importance of substrate selection in biological applications. Quantitative comparison of the various cellular interactions demonstrated that non-specific interactions can be much larger in magnitude than peptide- and protein-mediated adhesion. As adhesion is the first step in a cascade of events through which cellular interaction with a material surface occurs, this finding has implications on assays of long-term cellular function as well. The insight provided by these studies should help in the development of optimized protein and peptide microarrays, or biochips, as well as better bioactive materials for biomaterial/tissue engineering applications.

Keywords: Self-assembled monolayer (SAM); cell adhesion; model surface; spinning disc assay; non-specific effect; fibronectin; RGD.

[*]To whom correspondence should be addressed. Tel.: (1-215) 898-9824; Fax: (1-215) 573-2128; e-mail: markhl@alumni.upenn.edu

1. INTRODUCTION

Self-assembly represents a powerful and versatile strategy to create substrates with strictly controlled molecular-level physicochemical characteristics. Because of this, self-assembled monolayers (SAMs) of surfactants on inorganic substrates have been widely utilized to date in a multitude of applications in analytical chemistry, nanotechnology and biotechnology [1, 2]. In the biological disciplines, SAMs have been used to immobilize a wide variety of biomolecules, such as antibodies [3], enzymes [4], peptides [5–8] and DNA [9, 10], to fabricate biologically functional materials for both practical and fundamental studies of interactions at biointerfaces. The insight provided by these studies has been of great value in the development of microarrays, or biochips [11–13], as well as bioactive materials for biomaterial/tissue engineering applications [14].

Adhesion is the first step in a cascade of events through which cellular interaction with a material surface occurs and, thus, plays a critical role in determining subsequent cellular function. It is a complex phenomenon which is mediated by a combination of many overlapping interactions, including non-specific forces arising from the substrate's physicochemical characteristics and specific forces through binding events between physisorbed or chemisorbed biomolecules on the material surface and receptors on the cell surface. Furthermore, these events occur concurrently at different rates. Non-specific adhesion and protein adsorption onto the substrate occur immediately and are followed by slower receptor–ligand binding processes which provide specific intracellular cues to alter cell function. Despite the plethora of studies in the literature which address cellular adhesion, a quantitative understanding of the magnitude of these various interactions is currently lacking. It is the goal of this work to address this issue at the molecular level using silane SAMs as model functional substrates.

In previous studies, we had reported on the preparation and characterization of SAMs of 3-glycidoxypropyltrimethoxysilane (GPTMS), triethoxysilylpropyl succinic anhydride (TESPSA), 3-aminopropyltriethoxysilane (APTES) and octadecyltrichlorosilane (OTS) [8], and had employed them to study the correlation of a substrate's physicochemical properties with the efficacy of an adsorbed extracellular matrix (ECM) protein, fibronectin, in mediating cellular adhesion [8]. In this study, we characterize the functional groups present on these SAMs and the resulting dispersion, polar and hydrogen-bonding characteristics using fluorescence microscopy and four-liquid contact angle measurements. We also describe methods for chemically modifying the base SAMs to develop substrates for studying cellular adhesion. Namely, facile routes to fabricate OH-functional silane SAMs by modification of GPTMS and conjugation of arginine–glycine–aspartic acid (RGD) peptides to modified APTES SAMs are illustrated. Using these substrates, we examine the correlation between cellular adhesion and surface properties and show the dominant role that electrostatics plays in cellular adhesion. Lastly, we compare quantitatively the magnitudes of non-specific, protein- and peptide-

mediated cellular adhesion to demonstrate the relative roles that each plays in bio-interfacial interactions.

2. EXPERIMENTAL

2.1. SAM preparation

A 4-inch diameter silicon wafer (Silicon Quest, Santa Clara, CA, USA: p-type, <100> orientation, 20–30 Ω-cm resistivity) was cut into samples of 1.2 cm × 1.2 cm and were cleaned with piranha solution (7:3 (v:v) H_2SO_4/H_2O_2 (Fisher Scientific)) at 80°C for 20 min. After cooling to room temperature, the substrate samples were rinsed thoroughly with ultrapure water (Millipore Direct-Q, 18 MΩ-cm resistivity) and were stored under ultrapure water until use. The silicon substrates were then dried with N_2 and exposed to UV-Ozone (Jelight, Irvine, CA, USA: Model 42 UV-O Cleaner) for 10 min. Silane deposition was performed by immersion of the samples into a 5–20% (v:v) solution of the silane solution (Aldrich, Milwaukee, WI, USA or Gelest, Morrisville, PA, USA) in toluene or hexane for 16 h under the anhydrous conditions of a Unilab glovebox (MBraun, Stratham, NH, USA). The silane concentration was optimized for each SAM type: 3-glycidoxypropyltrimethoxysilane (GPTMS, 20%), triethoxysilylpropyl succinic anhydride (TESPSA, 10%), 3-aminopropyltriethoxysilane (APTES, 5%) and octadecyltrichlorosilane (OTS, 5%). For GPTMS, TESPSA and APTES, anhydrous toluene was used as the solvent during reaction and the samples were successively sonicated in toluene, N,N'-dimethylformamide (DMF) and water. For OTS, anhydrous hexane and chloroform were used in place of toluene and DMF, respectively. After fabrication, GPTMS was further modified to produce OH SAMs using two different treatments: (1) 100 mM HCl at 80°C for 1 h; and (2) 2.75 mM 2-mercaptoethanol (β-ME) in phosphate buffer solution (PBS, pH 7.4) at 25°C for 16 h. Both substrates were subsequently sonicated with ultrapure H_2O. GPT-OH denotes the β-ME-modified GPTMS SAMs.

APTES SAMs were immersed and sonicated in 5.0 mM solution of β-maleimidopropionic acid N-hydroxysuccinimide ester (BMPS) in acetonitrile (ACN) for 1 h, followed by successive sonication in acetonitrile, acetone, and ultrapure water (20 min each). Unreacted amines on the substrates were acetylated using a 1:1:1:2 molar solution of acetic acid/1-hydroxybenzotriazole (HOBt)/2-(1H-benzotriazole-1-yl)-1,1,3,3-tetramethyluronium hexafluorophosphate (HBTU)/N,N-diisopropylethylamine (DIEA) in DMF for 1 h. After sonication in DMF and water, the acetylation and sonication procedure was repeated once more. Lastly, these substrates were immersed in the peptide solution in Dulbecco's phosphate buffer solution (0.1 M sodium phosphate, 0.15 M NaCl, pH 7.2, Invitrogen, Carlsbad, CA, USA) for 1.5 h at room temperature. The concentration of the peptide solution was varied to achieve the same surface density (6 pmol/cm^2), as determined from radiolabeling results. RGD 1 denotes Acetyl–

Cys–Tyr–Gly–Gly–Arg–Gly–Asp–Ser (Ac-CYGGRGDS) and RGD 2 denotes Acetyl–Cys–Tyr–Gly–Gly–Arg–Gly–Asp–Ser–Val–Val–Tyr–Gly–Leu–Arg (Ac-CYGGRGDSVVYGLR). The unreacted maleimides were subsequently blocked using a 1 mM β-ME solution in PBS for 30 min. A two-fold molar excess of tris(2-carboxyethyl)phosphine (TCEP, Pierce Biotechnology, Rockford, IL, USA) was added to both the peptide and β-ME solutions to maintain the thiol groups in their reactive, reduced state.

For the biological experiments, all SAMs were rinsed successively, three times each, in 70% ethanol, ultrapure H_2O and PBS (pH 7.4) immediately prior to use. Unless otherwise noted, all reagents were used as received from Aldrich.

2.2. SAM characterization

Film thickness and homogeneity were determined using an AutoEl-II Null Ellipsometer (Rudolph Research, Flanders, NJ, USA) at a fixed incident angle of 70º with a helium-neon laser source ($\lambda = 632.8$ nm). All measurements were collected within 3–4 h of sample preparation to minimize contamination. Silicon oxide thickness was determined using a two-layer model with fixed refractive index of 1.462 and the SAM layer thickness was subsequently determined using a three-layer model with the following refractive indices: GPTMS = 1.429, TESPSA = 1.441 and APTES = 1.423 [15].

Surface topography and roughness were determined by atomic force microscopy (Digital Instruments, Santa Barbara, CA, USA: Dimension 3000 AFM) using the tapping mode with a single crystal Si tip with a resonant frequency of approx. 300 kHz. Height and phase images (1 μm × 1 μm area) were collected simultaneously and analyzed using the manufacturer-provided Nanoscope software.

All sessile drop contact angle measurements were taken using a goniometer setup built in-house containing a Hamilton microsyringe and a CCD camera. The typical protocol involved using a constant drop volume (approx. 10 μl) which was gently deposited onto the surface and the image collected. The captured images were analyzed using Scion Image program (Scion Corporation, Frederick, MD, USA) to determine the contact angles. A minimum of 30 separate readings were taken for each sample/probe liquid set and all readings were performed within 30 min of sample preparation to minimize contamination.

2.3. Cell culture and quantitative adhesion assay

Human K562/K100 erythroleukemia cells and murine NIH3T3 fibroblasts were grown in Dulbecco's modified Eagle's medium (DMEM, Invitrogen) supplemented with 10% calf serum (Invitrogen) using standard cell culture techniques. Bovine aortic endothelial cells (BAEC) and murine MC3T3 osteoblast-like cells were grown similarly in DMEM supplemented with 10% fetal bovine serum. The cells were centrifuged into a pellet and resuspended in serum-free DMEM and di-

luted to the appropriate concentration. For the fibronectin samples, the $\alpha_5\beta_1$ integrin receptors of the K562 cells were uniformly activated by the addition of TS2/16 monoclonal antibody [16] to the cell solution (1:5 dilution by volume) prior to seeding onto substrates for all experiments.

Circular silicon samples of 1 inch in diameter (Silicon Quest: p-type, <100> orientation, 20–30 Ω-cm resistivity) were prepared as previously mentioned and mounted on stages designed for the spinning disc device. The details of the device and protocol can be found elsewhere [17]. Briefly, 2.0×10^5 cells in 0.5–1 ml of buffer (24 mM HEPES, 137 mM NaCl, 2.7 mM KCl, 1 mM $MgCl_2$ and 1 mM glucose, pH 7.4) were placed onto the substrates. The cells were allowed to attach to the surface for 15 min at 37°C, the chamber was carefully filled with adhesion buffer and then the samples were spun for 5 min at an appropriate angular velocity to develop a good detachment profile. It should be noted that the time-scale of the experiment was restricted to focus on the early-stage cell–substrate adhesion. This protocol served to minimize complications due to deposition of endogenous proteins and cell spreading. Both of these events can significantly influence the observed attachment strength. The remaining cells were fixed with 1 ml of 3.7% formaldehyde solution in PBS for 10 min, permeabilized with 1% Triton-X for 10 min and stained with the fluorescent dye 4′,6-diamidino-2-phenyl-indol (DAPI) at 37°C for 20 min. The cell counting protocol was performed using an Optiphot fluorescence microscope (Nikon, Melville, NY, USA) with a Ludl XYZ stage and Ludl filter wheel/shutter (LUDL Electronics Products, Hawthorne, NY, USA) driven by ScopePro V1.0 software and a Photometrics SenSys cooled CCD camera. The data were analyzed using Image-Pro V 3.0 software to automatically count the number of cells at different radii from the center of the sample disc and SigmaPlot was used to sigmoidally curve-fit and analyze the data. It should be noted that 61 microscope fields (10×) were counted per sample (3–4 fields for a given radius on the sample disc) and that 10–20 samples were analyzed per sample type (from 3–5 separate experiments).

3. RESULTS AND DISCUSSION

3.1. Silanization and characterization

As the first step in producing model substrates for quantitative studies of cell adhesion, the protocol for self-assembly was selected and optimized to produce consistent, monolayer films with the expected physicochemical characteristics. The quality of the base SAMs was previously characterized by ellipsometry, AFM, water contact angle goniometry, and X-ray photoelectron spectroscopy (XPS). The ellipsometric thickness and root-mean-square (RMS) roughness of the SAMs were as follows: GPTMS (0.95 ± 0.1 nm, 0.27 ± 0.03 nm); TESPSA (0.87 ± 0.1 nm, 0.21 ± 0.03 nm); APTES (0.89 ± 0.1 nm, 0.24 ± 0.01 nm); OTS (2.63 ± 0.2 nm, 0.25 ± 0.03 nm) [8]. However, for many biological applications, direct in-

formation on functional group density and homogeneity is generally considered to be more important than the standard physicochemical characterization. Therefore, we further evaluated the functional groups present on the SAMs by conjugating them with fluorescent tags. Figure 1 shows a representative set of AFM surface scans and microscope images of fluorescein isothiocyanate (FITC)-conjugated APTES SAM and unmodified SiO_2. The images demonstrate that a highly dense and homogeneous array of functional groups is present on the SAM surface and that the SAM possesses similar sub-nanometer level roughness as the unmodified SiO_2 (approx. 0.2–0.3 nm for SAM *versus* 0.18 nm for SiO_2). As the physical features of substrates, such as roughness, are well known to influence cell adhesion and function [18], using model surfaces such as SAMs is critical in studying sensitive and complex biological phenomena. Similar results were also obtained by using a carboxyl-reactive fluorescent dye and TESPSA SAM. Direct and efficient labeling of the epoxide functional groups of GPTMS was not possible with commercially available fluorescent dyes.

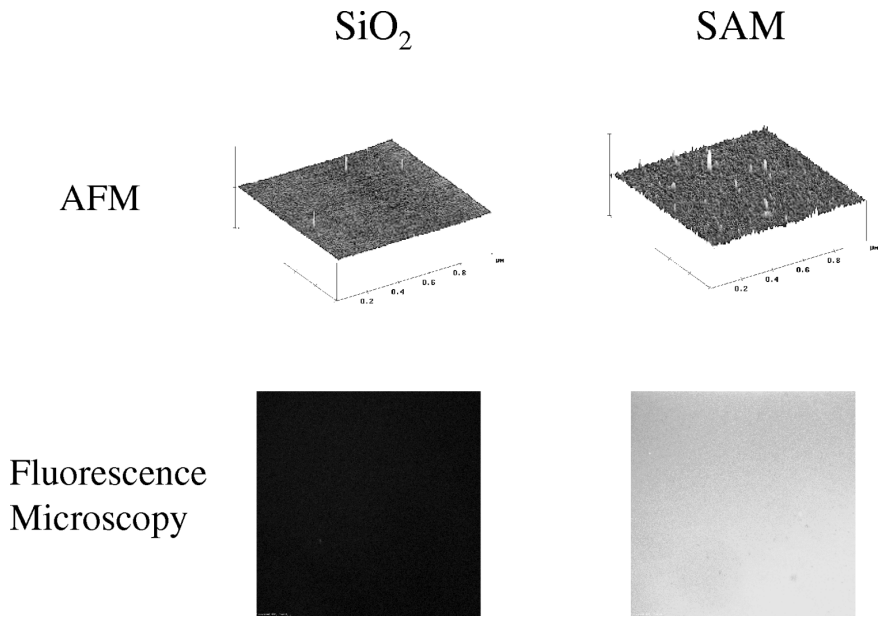

Figure 1. Characterization of the homogeneity of SAM substrates in comparison to SiO_2 using AFM and fluorescence microscopy. Height-mode AFM scans are over an area of 1 μm × 1 μm with a vertical scale of 10 nm/div. The RMS roughness value from the AFM images of SiO_2 was 0.18 ± 0.02 nm and of APTES was 0.27 ± 0.03 nm. SiO_2 and APTES samples were also labeled with fluorescein isothiocyanate (FITC) for fluorescence microscopy to verify functional group homogeneity, which is shown below.

3.2. Modification of GPTMS to produce OH SAMs

Hydroxyl-functional SAMs are of interest in biological applications for use as neutral surfaces which minimize both protein adsorption and non-specific interactions. However, it is difficult to fabricate them directly from silane coupling agents with a terminal OH functional group. Two potential routes for obtaining OH SAMs from modification of the epoxide-functional GPTMS SAMs were investigated (Fig. 2): (1) acid catalyzed ring opening reaction and (2) grafting of 2-mercaptoethanol (β-ME) moieties. Table 1 shows the ellipsometric thickness and water contact angle values for GPTMS and the two modified substrates. The thickness did not significantly change with the acid treatment, while it increased 0.3 nm with the β-ME treatment. Both changes are consistent with the expected dimensions of the molecules in the modified SAM. The contact angle values are in agreement with those previously reported for alkanethiol OH SAMs [19]. It is noteworthy that these modified SAMs are comparable to oligo(ethylene glycol) in structure and possessed similar protein-resistant properties when radiolabeled fibronectin was allowed to adsorb (plateau level approx. 20 ng/cm^2 of fibronectin).

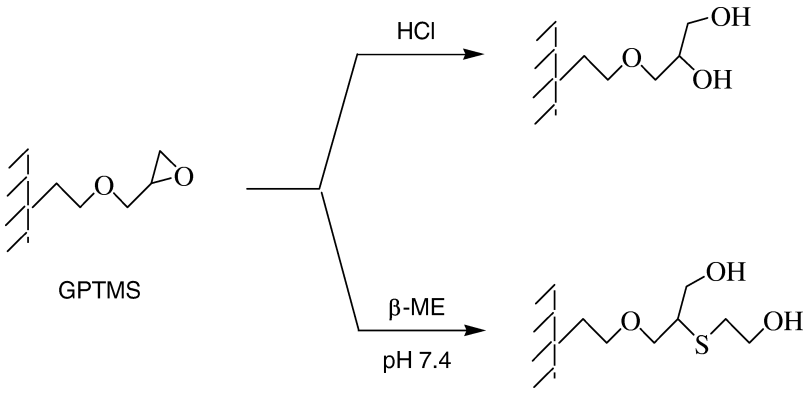

Figure 2. Modification of GPTMS to produce hydroxyl-terminated substrates. β-ME denotes 2-mercaptoethanol.

Table 1.
Ellipsometric thickness of and water contact angles on SiO_2, GPTMS and modified GPTMS substrates

Substrate	Thickness (nm)	Contact angle (º)
SiO_2	1.4 ± 0.0	0
SiO_2 + GPTMS	2.4 ± 0.1	44.3 ± 1.6
SiO_2 + GPTMS + HCl	2.3 ± 0.2	30.0 ± 5.6
SiO_2 + GPTMS + β-ME	2.7 ± 0.2	27.4 ± 3.7

As the two modifications to GPTMS yielded substrates of nearly identical characteristics, only the β-ME-modified GPTMS (GPT-OH) substrate was used for further experimentation.

3.3. Hydrolytic stability of SAMs

In considering silane SAMs for biological assays/applications, water stability is a key issue as most assays and applications are likely to expose the material to aqueous environments for extended periods of time. Although complete, well-formed monolayers would be optimal to minimize water penetration/hydrolysis of the anchoring siloxane bond, pinhole and defect-free films are rarely obtained in practice [1]. In addition, the silicon-oxygen bond is only 50% covalent in character and exists in a reversible hydrolysis equilibrium in the presence of water. This equilibrium reaction is illustrated in Scheme 1 and has an estimated equilibrium constant (K_{eq}) of approx. 10^{-5} [2]. By using tri-functional silanes, it was possible to impart excellent hydrolytic stability to the SAMs used in this work. The thickness of all well-formed SAMs decreased less than 0.1 nm when immersed in H_2O for all times tested (up to 18 h). However, it should be noted that poorly formed trialkoxysilane SAMs have been previously noted to very rapidly decrease in thickness (within 15 min) upon exposure to aqueous media [8]. This ultimately can lead to inconsistent measurements in assays of cellular adhesion and function. It should be noted that the stability of all SAMs used here was previously confirmed via ellipsometry [8] prior to the biological experiments.

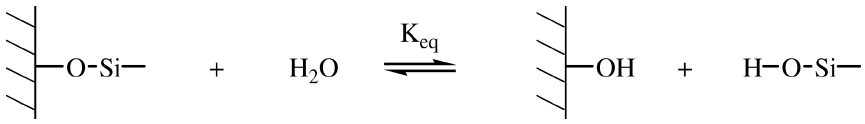

Scheme 1. Hydrolysis equilibrium of a monoalkylsilane bonded to hydroxylated inorganic substrates.

3.4. Contact angles on SAMs

In order to verify the substrate characteristics of the functional SAMs further, we also used contact angle goniometry with ultrapure water, formamide, glycerol and diiodomethane. By using these four distinct liquids in combination, it is possible to gauge separately a substrate's ability to interact at its surface through dispersion, polar and hydrogen bonding interactions. The characteristics of the four liquids and, therefore, the interactions that they are capable of probing, can be described using solubility parameters. The dispersion, polar and hydrogen bonding components of these parameters for the four liquids are listed in Table 2. Empirical relationships exist which more formally correlate solubility parameters with surface tension, which are more commonly used to describe surface energy, in some cases [26]. The liquids in increasing order of total surface energy are:

Table 2.
Hansen's solubility parameters of liquids used

Liquid	Solubility parameters ($MPa^{1/2}$)			
	δ_d	δ_p	δ_h	δ
Water	15.5	16	42.4	47.9
Formamide	17.2	26.2	19	36.6
Glycerol	17.4	12.1	29.3	36.2
Diiodomethane	17.8	3.9	5.5	19

Solubility parameter values are selected from Ref. [25]. Subscripts: d, dispersion component; p, polar component; h, hydrogen bonding component. Solubility parameters can be correlated with surface tension in some cases using empirical relationship: $\delta = 4.1\ (\gamma / V^{1/3})^{0.43}$ (non-polar liquids) [26]. γ, surface tension; V, molar volume.

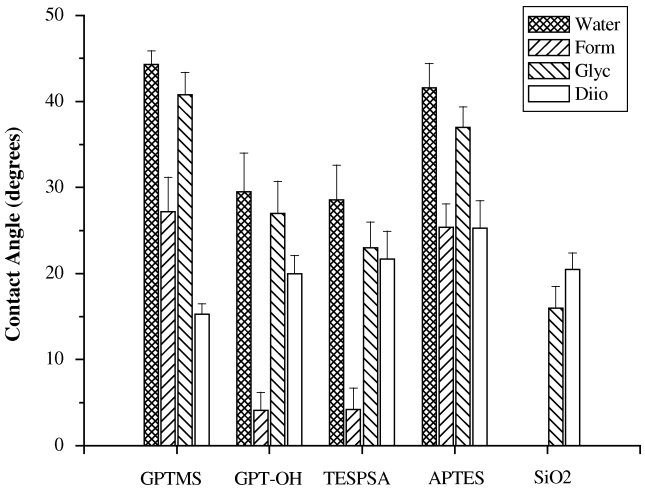

Figure 3. Contact angles of water, formamide, glycerol and diiodomethane on GPTMS, β-ME-modified GPTMS (GPT-OH), TESPSA, APTES and SiO_2. Values that are not displayed are below the measurement limit.

diiodomethane < glycerol ≈ formamide < water [20]. Despite having similar overall surface energy, formamide has a greater polar component while glycerol emphasizes hydrogen bonding interactions, as evident by their relative solubility parameter components. Diiodomethane probes only dispersion interactions as it does not possess any polar or hydrogen bonding characteristics.

Figure 3 shows the contact angles of all four liquids on GPTMS, β-ME-modified GPTMS, TESPSA, APTES and the unmodified SiO_2. Measurement of the contact-angle values on OTS for all four liquids was unncecessary since its water contact angle (103.4± 3.8º [8]) was significantly different from the other

substrates. The contact-angle values (θ) for water followed the expected general trend in hydrophilicity for the substrates based on the functional groups presented by the SAMs, namely, $\theta_{GPT\text{-}OH}$ (epoxide) ≈ θ_{TESPSA} (carboxyl) < θ_{APTES} (amine) < θ_{GPTMS} (epoxide) << θ_{OTS}. As the water–surface interaction is dominated by the hydrogen-bonding component, this result demonstrates a large hydrogen-bonding potential of the GPT-OH and TESPSA surfaces. The contact angle values of the substrates with formamide exhibited the trend: $\theta_{GPT\text{-}OH}$ (epoxide) ≈ θ_{TESPSA} (carboxyl) ≈ 0 < θ_{APTES} (amine) ≈ θ_{GPTMS} (epoxide). Therefore, GPT-OH and TESPSA have very high polar character as well. In comparison, APTES and GPTMS are both weakly polar substrates and exhibit finite contact angles. The trend in the contact-angle values for glycerol reinforces that found for water, since both surface–liquid interactions are dominated by the hydrogen-bonding component. Lastly, the contact-angle values with diiodomethane showed the following trend: θ_{GPTMS} (epoxide) < $\theta_{GPT\text{-}OH}$ (epoxide) ≈ θ_{TESPSA} (carboxyl) ≈ θ_{APTES} (amine). However, because the dispersion character of the terminal groups of the four SAMs is relatively weak, the contact angle for diiodomethane shows the smallest difference between sample types.

3.5. Conjugation of adhesive peptides to SAMs

A wide variety of strategies are used to attach biomolecules, such as peptides, to functional material surfaces. Functional groups which are commonly introduced by surface modification or by material design and used as anchoring points include –NH_2, –COOH and –SH groups. Because these groups are present in the structure of proteins, a wide array of cross-linking molecules are commercially available and generic protocols exist for many biological applications [21]. The two most common bioconjugate methods to biomaterials research to attach peptides and proteins to NH_2-functional APTES SAMs are the carbodiimide

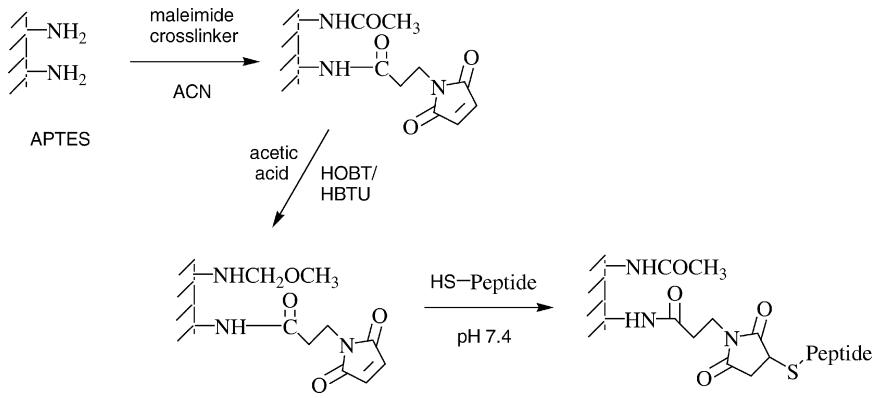

Figure 4. Conjugate chemistry used to attach peptides to 3-aminopropyltriethoxysilane (APTES) SAMs. Free NH_2 groups remaining on the substrate after the maleimide crosslinker step were blocked by acetylation. ACN denotes acrylonitrile.

activation of COOH groups of biomolecules and the conversion of NH_2 groups to maleimide functional groups. Since the former method may be complicated by side reactions between biomolecules themselves, the maleimide approach was used in this study. It is important to note also that the standard maleimide approach was modified to include an acetylation step to block any free, unreacted NH_2 groups before peptide-mediated cellular adhesion was measured. Figure 4 shows the coupling and acetylation reactions employed in this study.

3.6. Cell adhesion strength

In order to quantify the bio-specific and non-specific interactions involved in cellular adhesion, a spinning disc apparatus (SDA) was used for this work. A schematic illustration of the main components of the SDA and the hydrodynamic shear force generated by the apparatus are shown in Fig. 5. The linear relationship between shear stress and disc radius is significant as it allows the technique to sensitively detect differences in adhesion at low range of forces (e.g., due to receptor–ligand bonds) [22]. The raw data from the technique (number of cells that remain attached as a function of radius) are converted into "detachment profiles" in order to determine the shear stress at which 50% of the cells remain attached (τ_{50}). The τ_{50} value is a commonly used metric of adhesion strength and allows for the quantitative comparison of the adhesiveness of different substrates. A higher τ_{50} value is indicative of greater strength of cellular adhesion to the substrate. Figure 6 shows representative detachment profiles and τ_{50} values for two substrates of different adhesion characteristics as an example. Because the SDA is a population-based assay (as opposed to single cell measurements), the technique and the resulting τ_{50} values possess robust statistics.

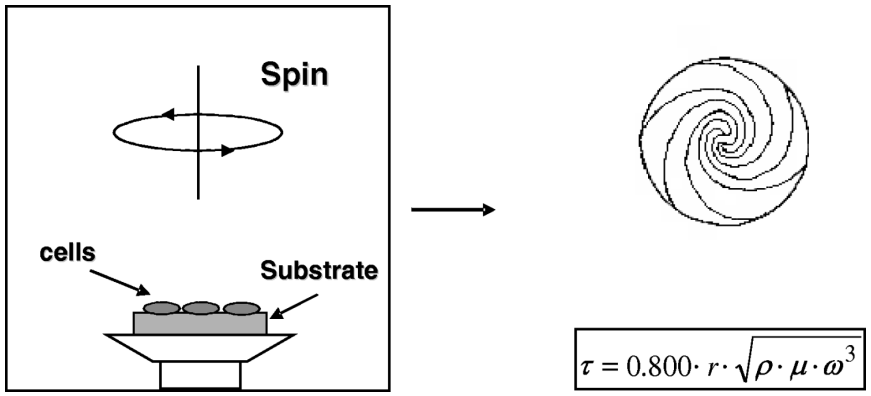

Figure 5. (left) Schematic illustration of the spinning disc apparatus used to quantify cellular adhesion. (right) The hydrodynamic profile (top view) generated on the disc allows for simultaneous application of a range of shear forces to detach cells. In the governing equation, τ, r, ρ, μ and ω represent the shear stress, radial distance of the cell, cell medium density, cell medium viscosity and the angular acceleration of the device.

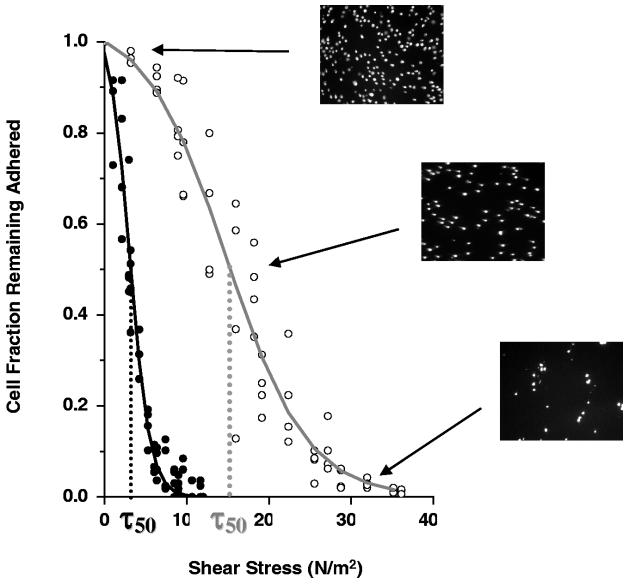

Figure 6. Representative cellular detachment profiles of two substrates of different adhesiveness from the spinning disc apparatus. Three representative microscopic images (10×) of the attached cells at the center (top), at an intermediate radius (middle) and at the edge (bottom) of the disc are shown as inserts. The solid lines are fits to the data used to determine the τ_{50} values which are used to compare the adhesive character of different substrates. The data shown are for K100 cells on sample of APTES (open circles, 16 N/m^2) and GPTMS (closed circles, 3.2 N/m^2).

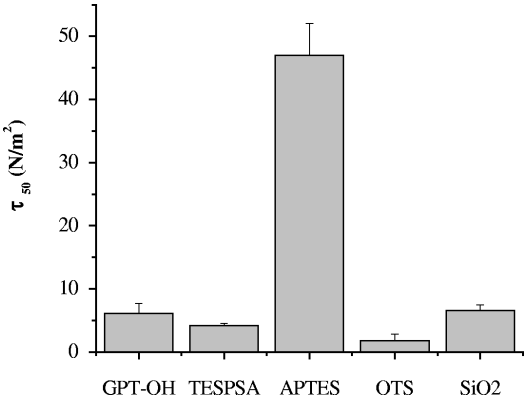

Figure 7. Detachment strength (τ_{50}) of MC3T3-E1 osteoblast-like cells to β-ME-modified GPTMS (GPT-OH), TESPSA, APTES, OTS and SiO_2. Error bars represent 95% confidence intervals.

The non-specific adhesion levels for the different SAMs were first investigated using MC3T3-E1 osteoblast-like cells (Fig. 7). A comparison of Figs 3 and 7 shows that the trend in cellular adhesion does not correlate simply with polarity or

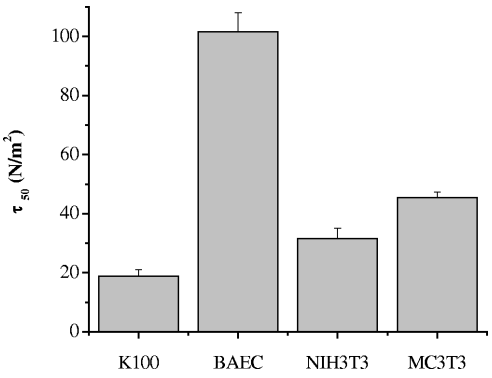

Figure 8. Detachment strength (τ_{50}) of various cells to APTES: K100 = Human erythroleukemia, BAEC = Bovine aortic endothelial cells, NIH3T3 = murine fibroblasts, MC3T3 = murine osteoblast-like cells. Error bars represent 95% confidence intervals.

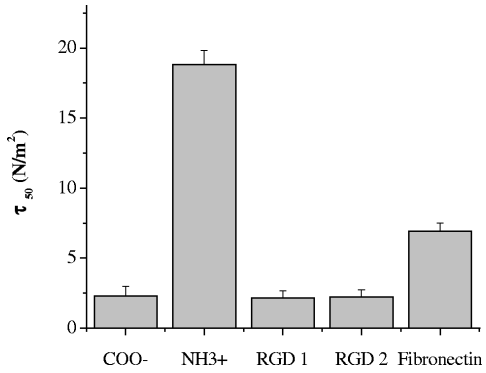

Figure 9. Comparison of the magnitudes of the non-specific (COO^-, NH_3^+), peptide-mediated (RGD 1, RGD 2) and protein-mediated (Fibronectin) adhesion of K100 cells. The values for RGD 1, RGD 2 and fibronectin represent the increase in adhesion from the unmodified control substrate (i.e., the specific adhesion only). Error bars represent 95% confidence intervals.

hydrogen bonding of the functional groups. An alternate interpretation is to consider cellular adhesion in the context of electrostatics and hydrophobicity. The reasoning for this lies in the fact that the surface of most mammalian cells is coated with a hydrated, negatively-charged carbohydrate layer known as the glycocalyx. In biological media (i.e., pH 7.2–7.4), APTES and TESPSA SAMs are essentially dense arrays of NH_3^+ and COO^- groups, respectively, and can interact electrostatically with the glycocalyx. This general interpretation is supported by the following findings shown in Fig. 7, namely: (1) the τ_{50} value for the APTES SAMs is dramatically larger (~10× than all other SAMs and SiO_2, (2) the τ_{50} value of TESPSA was lower than that of neutral surfaces (i.e., GPT-OH) and (3) OTS exhibited the lowest adhesion level of all substrates, likely due to repulsion

of the hydrated cell glycocalyx from the hydrophobic substrate (water contact angle = 103.4 ± 3.8º [8]). It should be noted that the relative trend among the different substrates was similar for all other cell types which were tested as well and suggests that this property–adhesion correlation may be somewhat universal. However, the magnitude of the electrostatic effect differed greatly between cell types (Fig. 8), presumably due to differences in the charge density or size/surface area of the different cells.

Lastly, we examined the magnitude of the electrostatic interactions arising from the charged silane SAMs in relation to specific ones mediated by adhesive ECM proteins and peptides. Quantitative understanding of the separate contributions of non-specific (such as electrostatic) and specific (such as those by receptor–ligand bonds) components of cell adhesion allows for a better correlation of differences in substrate adhesiveness with those in cell function, which are primarily mediated by specific interactions. K100 erythroleukemia cells were used for this part of the work because they represent simpler cell types without a complex adhesion response found in most other cell types (i.e., no cell spreading, no multiple receptor expression, etc.). Since grafted RGD peptides and physisorbed extracellular matrix (ECM) proteins, such as fibronectin, are extensively used in biomaterials research for the purpose of specifically increasing cellular adhesion, they are the appropriate substrates for comparison. In addition, a second peptide sequence containing the RGD sequence (RGDSVVYGLR) from another ECM protein, osteopontin, was included as well, since it is generally believed that longer peptides are more effective ligands. Figure 9 shows the τ_{50} values for TESPSA, APTES, two different RGD peptides (RGDS and RGDSVVYGLR) and adsorbed fibronectin of similar surface density (approx. 6 pmol/cm^2 as determined using radiolabeled peptides [23] and fibronectin [24]). The results show that the differences in non-specific adhesion due to substrate chemistry can be much larger in magnitude than the weak, specific ones mediated by adhesive peptides and proteins. As common blocking procedures used in biological research, such as adsorption of non-adhesive proteins, have been shown to be only partially effective in removing large non-specific effects [8], the importance of considering the functional groups introduced by substrate selection/surface modification and by biomolecule attachment chemistry is demonstrated.

4. CONCLUSIONS

Self-assembled monolayers (SAMs) of different surface functional groups were fabricated using commercially available silane coupling agents. These substrates were chemically modified to produce other biologically relevant surfaces (such as OH SAMs) and to attach or adsorb biomolecules (such as RGD peptides and fibronectin). Interactions between cells and SAMs did not correlate simply with substrate's properties such as polarity and hydrogen bonding ability but instead were significantly influenced by electrostatic interactions. Attractive interactions

from positively-charged substrates, such as those with NH_3^+-functional groups (APTES at physiological pH), dominated the non-specific adhesion of cells. This was found for a variety of cell types tested in this work and may be universal for mammalian cells. In order to determine the relevance of the non-specific effects in the context of biomaterials and biotechnological applications, a quantitative comparison of the large electrostatic interaction with RGD peptide- and fibronectin-mediated adhesion was performed. The results showed that the former interaction introduced from substrate chemistry alone can dominate the weak, specific interactions of the latter. Thus, this study shows quantitatively that non-specific interactions can be a significant component in cellular adhesion. Therefore, proper selections of the substrate and of the bioconjugate chemistry used to attach biomolecules are both critical considerations in designing studies of cellular interactions at interfaces.

Acknowledgements

This research was supported by NIH (DE-13009) and NSF (IGERT Fellowship in Nanoscale Science & Engineering: DGE-0221664).

REFERENCES

1. A. Ulman, *An Introduction to Ultrathin Organic Films: From Langmuir-Blodgett to Self-Assembly*. Academic Press, Boston, MA (1991).
2. E. P. Plueddemann, *Silane Coupling Agents, 2nd edn*. Plenum, New York, NY (1991).
3. S. K. Bhatia, L. C. Shriver-Lake, K. J. Prior, J. H. Georger, J. M. Calvert, R. Bredehorst and F. S. Ligler, *Anal. Biochem.* **178**, 408-413 (1989).
4. D. A. Puleo, *J. Biomed. Mater. Res.* **29**, 951-957 (1995).
5. S. P. Massia and J. A. Hubbell, *Anal. Biochem.* **187**, 292-301 (1990).
6. S. J. Xiao, M. Textor, N. D. Spencer, M. Wieland, B. Keller and H. Sigrist, *J. Mater. Sci.: Mater. Med.* **8**, 867-872 (1997).
7. A. Rezania, R. Johnson, A. R. Lefkow and K. E. Healy, *Langmuir* **15**, 6931-6939 (1999).
8. M. H. Lee, D. A. Brass, R. Morris, R. J. Composto and P. Ducheyne, *Biomaterials* **26**, 1721-1730 (2005).
9. L. A. Chrisey, G. U. Lee and C. E. O'Ferrall, *Nucleic Acids Res.* **24**, 3031-3039 (1996).
10. R. Lenigk, M. Carles, N. Y. Ip and N. J. Sucher, *Langmuir* **17**, 2497-2501 (2001).
11. M. Schena, *Microarray Biochip Technology*. Eaton, Natick, MA (2000).
12. R. Michel, J. W. Lussi, G. Csucs, I. Reviakine, G. Danuser, B. Ketterer, J. A. Hubbell, M. Textor and N. D. Spencer, *Langmuir* **18**, 3281-3287 (2002).
13. B. T. Houseman, E. S. Gawalt and M. Mrksich, *Langmuir* **19**, 1522-1531 (2003).
14. M. Mrksich, *Chem. Soc. Reviews* **29**, 267-273 (2000).
15. Metal Organics for Material & Polymer Technology: *Supplement to the 2001 Gelest General Catalog* (2001).
16. E. Van de Wiel-Van Kemenade, Y. Van Kooyk, A. J. De Boer, R. J. F. Huijbens, P. Weder, W. Van de Kasteele, C. J. M. Melief and C. G. Figdor, *J. Cell Biol.* **117**, 461-470 (1992).
17. A. J. Garcia, P. Ducheyne and D. Boettiger, *Biomaterials* **18**, 1091-1098 (1997).
18. R. G. Flemming, C. J. Murphy, G. A. Abrams, S. L. Goodman and P. F. Nealey, *Biomaterials* **20**, 573-588 (1999).
19. B. G. Keselowsky, D. M. Collard and A. J. Garcia, *J. Biomed. Mater. Res.* **66A**, 247-259 (2003).
20. L.-H. Lee, *Langmuir* **12**, 1681-1687 (1996).

21. G. T. Hermanson, *Bioconjugate Techniques*. Academic Press, San Diego, CA (1996).
22. A. J. Garcia, J. Takagi and D. Boettiger, *J. Biol. Chem.* **273**, 34710-34715 (1998).
23. M. H. Lee, C. S. Adams, D. Boettiger, W. F. DeGrado, I. M. Shapiro, R. J. Composto and P. Ducheyne, *J. Biomed. Mater., Res.* submitted.
24. M. H. Lee, P. Ducheyne, L. Lynch, R. J. Composto and D. Boettiger, *Biomaterials* **27**, 1907-1916 (2006).
25. J. Brandrup and E. H. Immergut (Eds.), *Polymer Handbook*. Wiley, New York, NY (1989).
26. J. H. Hildebrand and R. L. Scott, *The Solubility of Nonelectrolytes, 3rd edn*. Reinhold, New York, NY (1950).